1-2020

Object Identification in Radar Imaging via the Reciprocity Gap Method

Matthew Charnley

Aihua W. Wood
Air Force Institute of Technology

Recommended Citation

Charnley, M., & Wood, A. (2020). Object identification in radar imaging via the reciprocity gap method. Radio Science, 55(1). https://doi.org/10.1029/2019RS006946

Radio Science

RESEARCH ARTICLE
10.1029/2019RS006946

Special Section:
Special Issue of the 2019 URSI Asia-Pacific Radio Science Conference

Object Identification in Radar Imaging via the Reciprocity Gap Method

Matthew Charnley[1] and Aihua Wood[2]

[1]Department of Mathematics, Rutgers University, Piscataway, NJ, USA, [2]Department of Mathematics and Statistics, Air Force Institute of Technology, Wright-Patterson AFB, OH, USA

Key Points:
- Use of Lippmann-Schwinger equation and reciprocity gap approach for near-field object detection
- Permittivity identification using the Lippmann-Schwinger equation

Correspondence to:
M. Charnley,
charnley@math.rutgers.edu

Citation:
Charnley, M., & Wood, A. (2020). Object identification in radar imaging via the reciprocity gap method. *Radio Science*, *55*, e2019RS006946. https://doi.org/10.1029/2019RS006946

Received 12 AUG 2019
Accepted 15 DEC 2019
Accepted article online 21 DEC 2019

Abstract In this paper, we present an experimental method for locating and identifying objects in radar imaging, specifically problems that could arise in physical situations. The data for the forward problem are generated using a discretization of the Lippmann-Schwinger equation, and the inverse problem of object location is solved using the reciprocity gap approach to the linear sampling method. The main new development in this paper is an exploration of determining the permittivity of the object from the back-scattered data, utilizing another discretization of the Lippmann-Schwinger equation.

1. Introduction

Work on through-the-wall imaging has developed substantially over the last few years. Initial work in Keith (2013) developed a method to determine the characteristics of a person from back-scattered electromagnetic data in the through-the-wall case. More recent work in (Adib et al., 2015; Zhao et al., 2018) used a similar approach to get more detailed results, using the back-scattered data to estimate the pose of a human figure behind a wall or detect that the figure is walking toward the sensor. All of these results use a Support Vector Machine approach, which needs to be trained on known data before it can predict the type, pose, or location of figures from through-the-wall data.

Our previous work (Charnley & Wood, 2016, 2017) looks to develop a more direct approach to reconstructing the object, which led us to the linear sampling method (LSM) and, in particular, the reciprocity gap approach to it. The LSM has been shown to be an efficient way to locate an object using scattered data from all sides of the object (Cakoni & Colton, 2014). The reciprocity gap approach modifies calculations in the LSM to apply to point source incident fields instead of plane waves. Thus, this approach presents the potential of near-field application of the LSM as opposed to the original method, which is only applicable in the far field (Colton & Haddar, 2005). Our previous work shows that, even though some of the assumptions of the LSM are not met, this method still does a decent job locating and reconstructing objects in the through-the-wall setting. This paper expands on this development.

In Charnley and Wood (2016), we utilized the Yee Scheme to generate the forward problem data by solving the time domain Maxwell's equations. Since the LSM and the reciprocity gap approach in two dimensions make use of the reduction of TM or TE polarized Maxwell's equations to the Helmholtz equation, it would make more sense to utilize a method that generates a solution to the Helmholtz equation directly instead of relying on modifying a monochromatic solution to the wave equation to give a solution to the Helmholtz equation. The Lippmann-Schwinger equation provides an integral equation that the solution of the Helmholtz equation must satisfy (Kress, 2010). In order to generate a solution to the Helmholtz equation, we can discretize this integral equation and find an approximate solution on the grid points that are contained in the object and then extend this solution to the receivers that we want. There have been many developments to generate improved methods to solve the Lippmann-Schwinger equation (Ambikasaran et al., 2016). Here we choose to use a straightforward discretization for simplicity.

In addition to enhancing our previous work on the forward problem, here we also expand the inverse problem by developing a method for approximating the electrical permittivity of the object from back-scattered data. It has been shown in previous work that the eigenvalues of the interior transmission problem can be used to solve for this parameter (Cakoni et al., 2010; Giovanni & Haddar, 2012). In our case, we use a more direct numerical approach. The Lippmann-Schwinger equation suggests that the solution at the receivers should change with the coefficient in the Helmholtz equation, which depends on both frequency and the

permittivity of the object. In particular, it describes exactly how the field at the receivers depends on the material properties of the object. This allows us to compare the scattered data from an unknown object to those of known objects so as to determine the material parameters of an unknown object.

The rest of this paper is organized as follows. Section 2 outlines the numerical method developed here for generating the forward problem data, as well as the implementation of the reciprocity gap formulation of the LSM. Section 3 describes the process we use to approximate the permittivity of the object from the back-scattered data. Section 4 presents numerical experiments for the reconstructions of shape and location, as well as the permittivity identifications. Section 5 summarizes the results and discusses potential for future work.

2. Numerical Implementation

2.1. Lippmann-Schwinger Equation

The Lippmann-Schwinger equation is an integral formulation of the Helmholtz equation when used to analyze scattering problems. A solution u to

$$\begin{aligned} \Delta u + k^2 n(x) u &= 0 \qquad \mathbb{R}^2 \\ u &= u^s + u^i \\ \lim_{r\to\infty} \sqrt{r}\left(\frac{\partial u^s}{\partial r} - iku^s\right) &= 0, \end{aligned} \tag{1}$$

is a solution to the integral equation

$$u(x) = u^i(x) - k^2 \int_{\mathbb{R}^2} \Phi(x,y) m(y) u(y) \quad \mathrm{d}y \qquad x \in \mathbb{R}^2, \tag{2}$$

where $m = 1 - n$ and $\Phi(x,y) = \frac{i}{4} H_0^1(k|x-y|)$ is the fundamental solution to the background Helmholtz equation

$$\Delta u + k^2 u = 0.$$

This relationship is an equivalence provided m has compact support in $\mathbb{R}^2$, and all of the appropriate solutions are smooth enough (Cakoni et al., 2016). In particular, if m has support D, we notice that based on the formulation of (2), once we know the solution u on D, we can then extend the solution to any point in $\mathbb{R}^2$ by evaluation of the integral. For our particular formulation, we have that the index of refraction n is 1 everywhere except on the support of the object we are trying to locate. Thus, our support D is exactly the object that we are trying to find, and the integral equation tells us that the scattered field is known once we know the full solution on the object. The form of (2) also suggests the potential to restrict this to an operation on $L^2(D)$, which is how we proceed with generating the data for the forward scattering problem.

The Lippmann-Schwinger Equation (2), rewritten as an operator on $L^2(D)$ is given by

$$u^i(x) = u(x) + k^2 \int_{\mathbb{R}^2} \Phi(x,y) m(y) u(y) \quad \mathrm{d}y = (I + k^2 K) u \qquad x \in D, \tag{3}$$

where K is the integral operator on $L^2(D)$ with kernel $\Phi(x,y)m(y)$ for each fixed x in D. The domain D can be discretized, turning (3) into a matrix equation where the left-hand side represents the known source term, which is a point source away from D. This equation can then be solved by least squares methods. Some extra care needs to be taken when discretizing the integral term, as the kernel $\Phi(x,y)m(y)$ is singular at $x = y$, however, asymptotics of the Bessel functions show that it is integrable, and the diagonal terms in the matrix equation can be replaced by the appropriate evaluated integrals on a square around the singularity.

2.2. Forward Data Generation

The above discussion gives a fairly straightforward way to solve the forward problem: discretize the entire region, find the points that are in the support of m, solve this matrix equation, and then use (2) to compute the value of u at the locations where we want to measure the field. However, when the support of m is large and the incident field has high frequency, the size of this matrix equation can make it infeasible to solve. In addition, this matrix is dense, so it is impossible to leverage sparsity in order to store the matrix more efficiently. This is particularly likely to be the case in the through-the-wall setting, where the walls also contribute to the scattering phenomenon and need to be included in the support D. In order to deal with

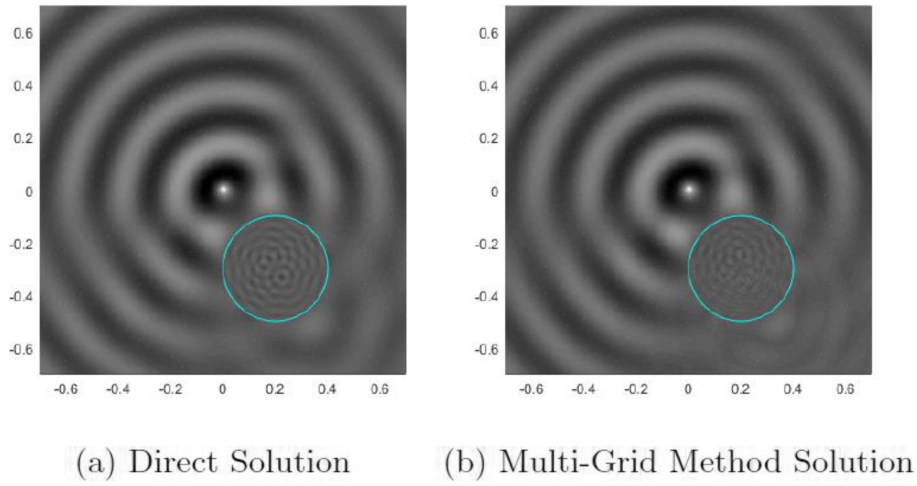

Figure 1. Comparison of (a) direct solution to (b) multigrid method.

this issue, we developed a multigrid-type scheme that allows us to solve the problem on coarser grids (where we have enough memory to store the entire matrix that we need to solve) and then extend the solution to finer grids using conjugate-gradient methods. These methods take significantly more time to run than direct solution methods, because as we cannot store the entire matrix equation that we need to solve, all of the matrix-vector multiplication operations in the conjugate-gradient part of this process must be done one element at a time. However, the fields generated by this method are similar, at least far from the scatterer, to those from the direct solution method. The experiment in Figure 1 compares the same solution u generated by the direct solution method and the multigrid method and shows how the two methods relate.

Remark. Our multigrid method only goes from coarser grids to finer grids without cycling the errors back to the coarse grid for direct solution (as would be done in a Full Multigrid scheme). Experiments showed that this process introduced a large disparity in the fields, and so the computation scheme was simplified to only a single V-cycle. We believe this discrepancy is caused by the errors of the solution with larger eigenvalues being eliminated in the conjugate-gradient method, so that only those with small eigenvalues are left, which would cause a large field to appear when inverting the matrix. This is a future point of study for this project.

For all of the examples presented below except where specifically indicated, the object was chosen small enough so that the multigrid method was not needed, and the forward problem can be solved by direct methods.

2.3. Reconstruction Method

The reconstruction method we use here follows our previous paper (Charnley & Wood, 2017), which uses the reciprocity gap formulation of the LSM discussed in Colton and Haddar (2005). As our incident field is a point source instead of a plane wave, this gives us a way to still use the ideas of the LSM for reconstruction.

The main modification made in this paper to the source/receiver array in Charnley and Wood (2017) is that the sources and receivers are now evenly spaced around concentric circles with center in the middle of the "room" as opposed to on squares. This allows for a simplification of the coding procedure, but the method would be able to handle any arrangement of sources and receivers. In addition, all of the examples done here are done in the free scattering setting, as opposed to through-the-wall, but we still constrain the objects to be in a specific region of $\mathbb{R}^2$. Examples of this reconstruction are shown in section 4.

3. Permittivity Identification

3.1. Methodology

The next thing we want to do is learn more about this object from the scattered data. We would like to use these data to determine something about the material parameters of this object, ideally being able to identify the type of material from which it was made. As the LSM only seeks to find the support of $m = 1 - n$, it does not give us any information about the actual values of n, which is the material parameter we are trying to determine here.

To develop our method for this, we first consider how the data for the forward problem is generated. In that case, we know the support and material properties, and given this information, we use the Lippmann-Schwinger equation to first find the value of the solution u on the object and then move it out to the receivers. The idea is to use the data generated from the LSM to find the support of the object, and then, assuming that this is the exact support of the object, calculate what the scattering data would be with an undetermined permittivity. If the permittivity of the object is changed, the scattered field will also change, and the error between this predicted scattered field and the one we measure should be minimized when the permittivity selected matches what the permittivity of the object was during the original solution of the forward problem. Therefore, we can use this method to approximate what the permittivity of the object is by minimizing this error. In particular, we will assume that the contrast m is constant on D, which allows us to simplify the calculations.

To be more precise, we define an operator $T : L^2(D) \to L^2(D)$ by

$$Tu(x) = k^2 \int_D \Phi(x, y)u(y) \quad \mathrm{d}y,$$

and an operator $B : L^2(D) \to L^2_{\mathrm{loc}}(\mathbb{R}^2)$ by

$$Bu(x) = -k^2 \int_D \Phi(x, y)u(y) \quad \mathrm{d}y.$$

These operators are almost identical, but they will be used in two different contexts for this problem. By combining these operators and using (2) and (3), we can see that the measured scattered field u^s satisfies, for the correct constant contrast m,

$$u^s = mB(u|_D) = mB\left((I + mT)^{-1}u^i\right).$$

In writing the equation this way, we assume that m is constant within the scatterer, so that it can be moved outside of all of the necessary integrals. However, we do not necessarily know the exact support D of the scatterer, which would allow us to numerically define the operators B and T. The LSM gives us an approximate support $\tilde{D}$, which we can use to define operators $\tilde{B}$ and $\tilde{T}$ where the integrals are defined over $\tilde{D}$ instead of D and compute a predicted scattered field $\tilde{u}^s$ as a function of the contrast m as

$$\tilde{u}^s(m) = m\tilde{B}\left((I + m\tilde{T})^{-1}u^i\right).$$

Finally, to attempt to classify the permittivity, we minimize error

$$m_{\mathrm{obj}} = \mathrm{argmin} \quad ||u^s - \tilde{u}^s(m)||,$$

where, in this case, the norm is an L^2 error across a set of sources and receivers.

3.2. Results and Permittivity Identification

For the numerical implementation of this method, we need to first generate the approximate support $\tilde{D}$. This is done by choosing a fractional cutoff α based on experimental results, running the LSM, and picking $\tilde{D}$ to be the set of all points where the value of the indicator function G, after averaging over a set of frequencies, is larger than α times the maximum value of G. Using this support, we can define operators $\tilde{T}$ and $\tilde{B}$ that will allow us to compute the scattered field from any incident data. We then pick a subset of the sources and receivers, and for each of these, compute the approximate scattered field $\tilde{u}^s$. It would be possible to use all of the sources and receivers, but since we are only trying to determine one parameter, we can still get an effective reconstruction with fewer of them. Finally, we can sum the error from each of the source-receiver pairs and minimize this total error in m.

To test out this method, we ran experiments to determine the permittivity of the object assuming we had the exact operators B and T instead of $\tilde{B}$ and $\tilde{T}$. Ideally, the method should return the correct contrast with zero error, but this was not the case, particularly with high-frequency data. Our conclusion was that the grid size we were using for the LSM was too coarse to accurately model the solution on the object at high frequency, which produced a significant error when calculating the scattered field as a function of m. However,

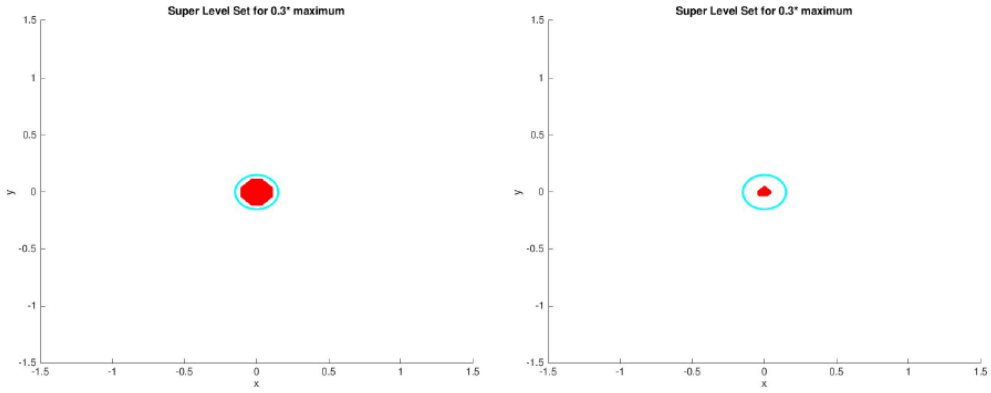

Figure 2. Reconstruction from (a) direct solution and (b) multigrid method

low-frequency data could not give an accurate reconstruction of the support of the object from the LSM for smaller objects, as the wavelength was too large. To fix this shortcoming, we decided to use two different sets of scattered data, one at high frequency to determine the support of the object and one at low frequency to determine the permittivity from this data.

Now, for the low-frequency data, if we take the exact operators B and T, the contrast is recovered almost exactly. There is a small variation in frequency, but it is close enough to identify the material from a list. For the approximate operators $\tilde{B}$ and $\tilde{T}$, the results are less ideal. Since the LSM does not generate the support of the object exactly, it has a hard time reconstructing the appropriate contrast. If the object is centered inside of the set of sources and receivers, then the reconstruction is fairly accurate but still does fluctuate with contrast. This, in particular, causes a problem when an object with higher contrast produces a reconstruction that is slightly larger than the actual object. When the minimization is then carried out, the process predicts a smaller contrast than desired because a larger object with smaller contrast will provide a similar scattering pattern to a smaller object with larger contrast. Since the LSM cannot say anything about the particular values of the contrast, it is strange that it should play a role in the reconstruction, in particular, how accurate the reconstruction is. Why this changes things is something that could be looked into in the future.

The two object reconstructions shown below are both at the center of the circles of sources and receivers. Based on numerical results, having the object off-center caused issues with the reconstruction, particularly with the reconstructed object being elongated toward the center of this circle. This would not be terrible in general, but it causes a lot of problem when mixed with the permittivity identification method proposed above. We believe that this is caused by the fact that we are dealing with near-field data, so the object being

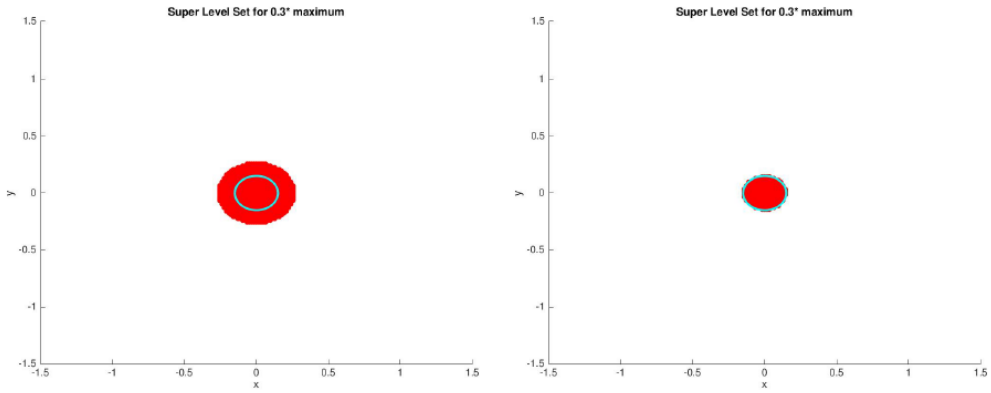

Figure 3. Support constructed for Object 1 at (a) low and (b) high frequencies.

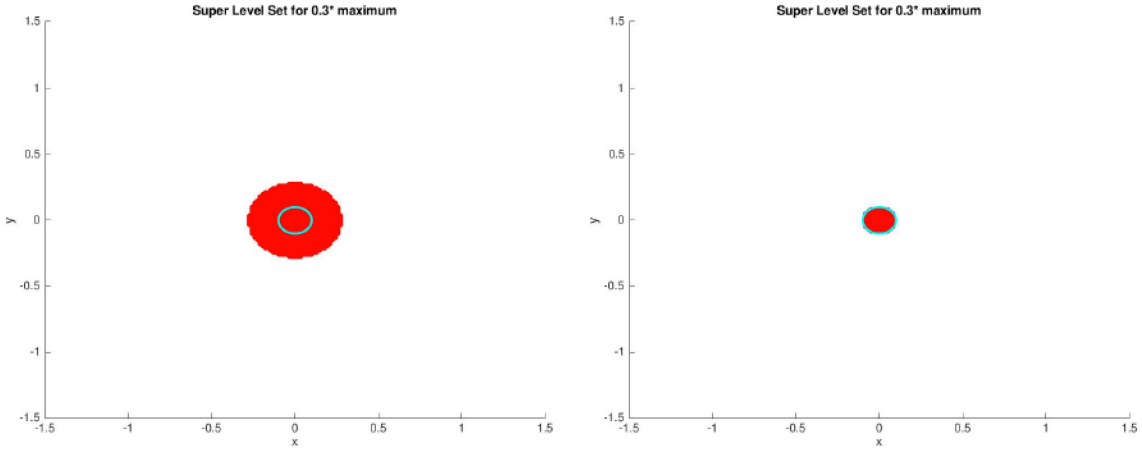

Figure 4. Support constructed for Object 2 at (a) low and (b) high frequencies.

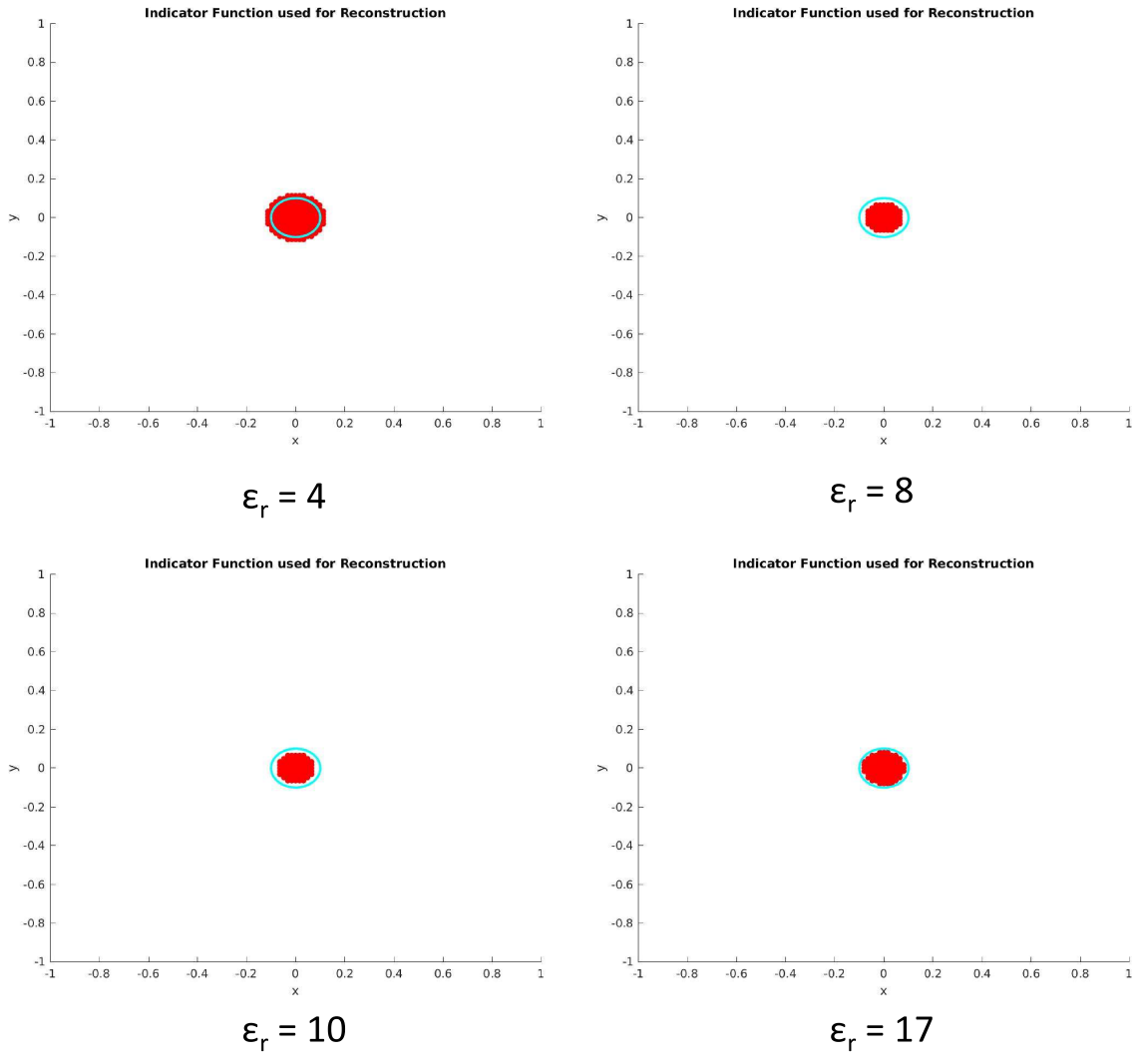

Figure 5. Reconstructions of the object for a variety in permittivities.

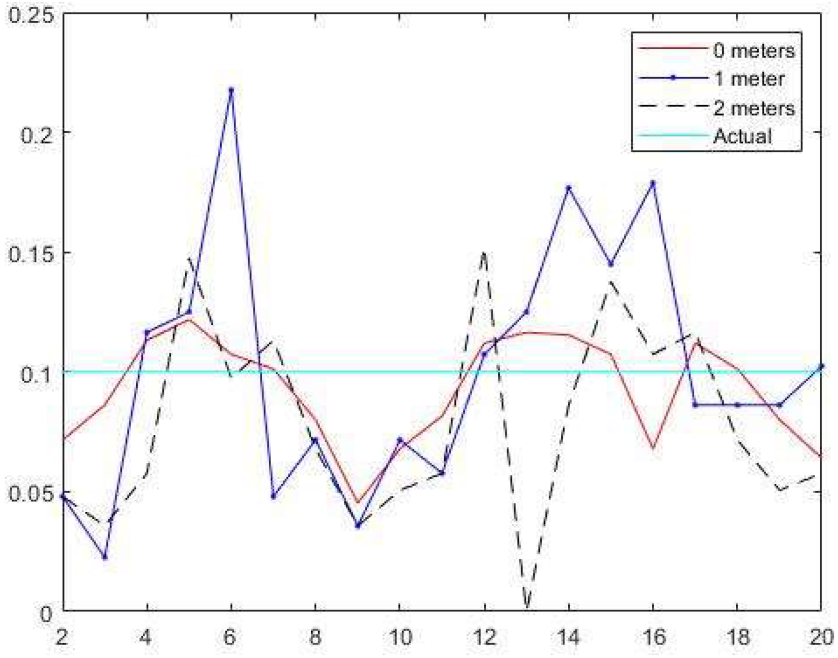

Figure 6. Graph of the reconstructed radius as a function of permittivity from different distances.

off-center causes a meaningful change in how the reconstruction method (which is meant for use in the far field) is carried out. In order to analyze the effect this has, we chose to do the reconstructions for the centered objects at three different distances and compare the results. The full analysis of how this works with off-center object reconstructions is a possibility for future work.

4. Computational Results

4.1. Multigrid Method

Figure 2 compares the reconstruction results from the direct solution and multigrid methods.

The reconstructions in Figure 2 are fairly different; however, the reconstruction done with the multigrid method still manages to find the location of the object. It does not do as well at determining the size of the object (which would cause significant problems in carrying out the permittivity determination described later) but shows at least some promise for locating larger objects. As mentioned previously, all of the remaining results will not use the multigrid method, but this would be necessary for handling larger objects and rooms with walls. Using this method does result in a different support, which would mean that more effort needs to be put into developing and formulating this method so that it can work more accurately.

4.2. Object Reconstruction

Now, we show how the methods described above can be used to reconstruct the support of the object along with its material parameters. Figures 3 and 4 illustrate the support $\tilde{D}$ constructed via the LSM as described above at both high and low frequencies.

As can be seen from Figures 3 and 4, the high-frequency data do a much better job of identifying the support of the object, particularly in the case of small objects. Therefore, we will use the data from the high-frequency calculations in order to determine the support for the material parameter reconstruction.

In doing the reconstruction, we noticed that the size of the reconstructed object, and thus the reconstructed object permittivity, did not consistently match over a range of permittivities. The plots in Figure 5 showcase this, where at different permittivities, the reconstructed object is a different size.

Figure 6 shows the radius of the reconstructed object as a function of relative permittivity. Here, we varied the permittivity of the object between 2 and 20. The three lines on this graph indicate putting the sources and receivers at three different distances from the object: 0 m (which would be right on the edge of the room), 1 m away, and 2 m away.

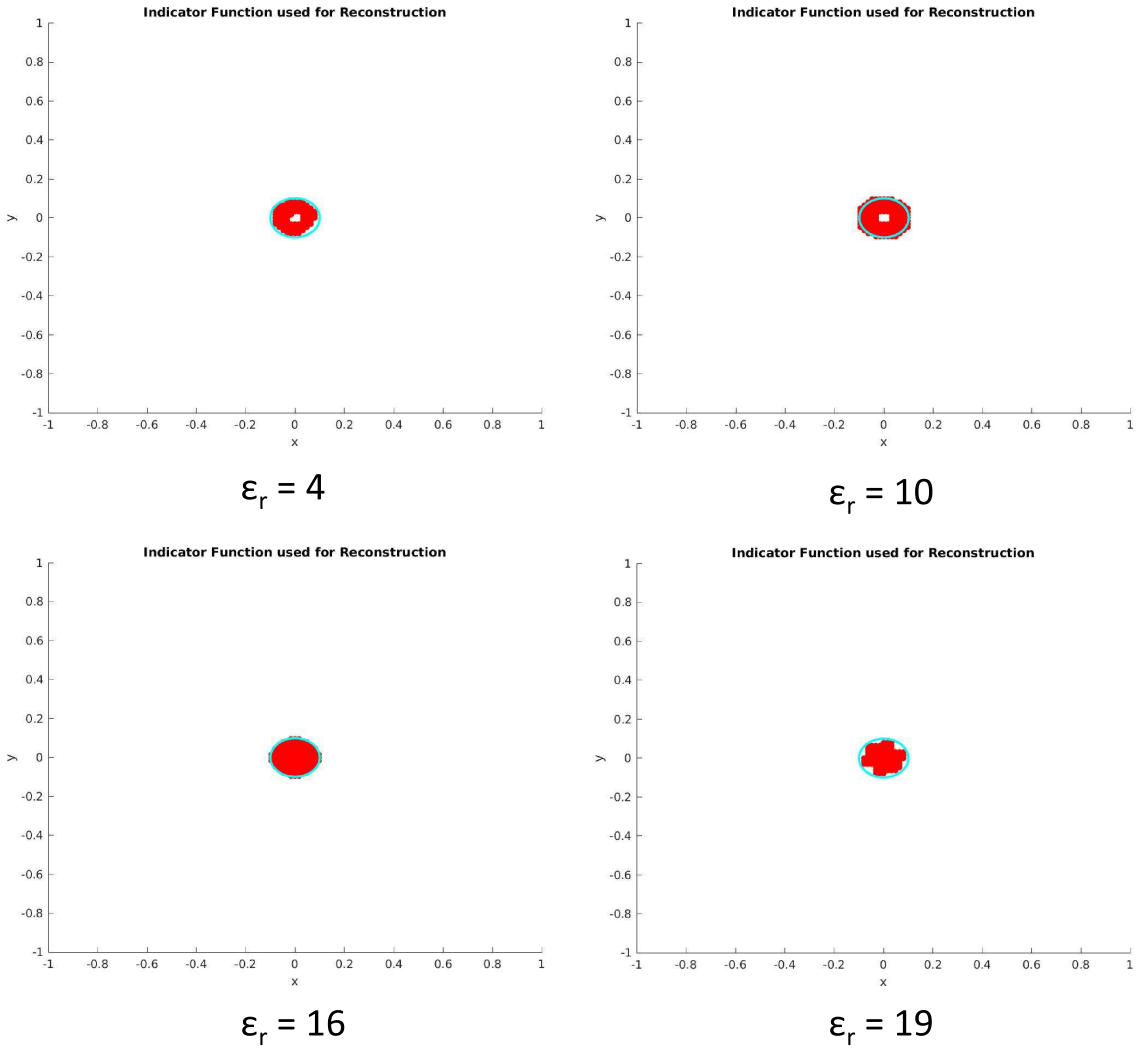

Figure 7. Reconstructions of a rough object for a variety of permittivities.

As can be seen in Figure 6, the reconstructed radius does not seem to depend in a predictable way on the permittivity. However, in general, it does seem that the reconstructed conductivity does follow the same pattern for each of the three different distances tested. Thus, more experiments could be used to figure out if this can be predicted and how to more accurately reconstruct the object.

In addition, we looked into how a rough object would affect this reconstruction method. To do this, we took our original data generation method, which used a subpixel smoothing technique to ensure smoothness of the permittivity function (Charnley & Wood, 2016, 2017), and removed the extra smoothing. Instead of smoothing out the function, we elected to replace the permittivity on these boundary pixels by a random decimal between 1 and the permittivity of the object. This would serve to model a boundary with roughness on the order of the grid spacing. Figure 7 shows the reconstructed object for a variety of permittivities, and Figure 8 shows the graph of reconstructed radius versus permittivity over the range from 2 to 20. As before, the three different distances for the locations of the sources and receivers are shown.

The graph we see in Figure 8 actually looks slightly better than the one in Figure 6. The spread of values is much lower, and the reconstruction radius is more consistent over the range of permittivities tested. The radius still does not seem to be predictable, and future experiments could lead more toward this goal. In addition, it seems like surface roughness on the order of pixel width does not harm the reconstruction using this method. It is possible that a larger roughness would have a negative effect on reconstruction, but that was not tested here.

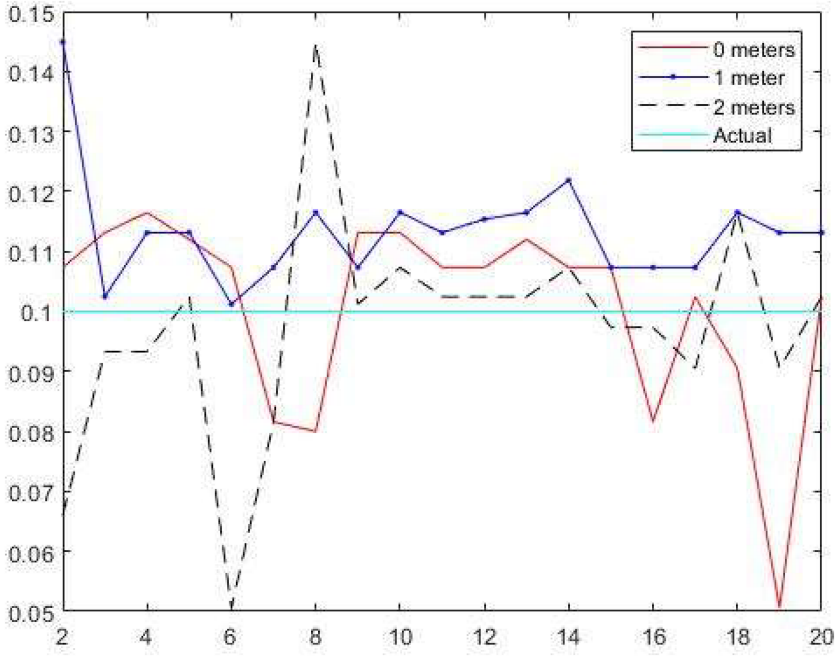

Figure 8. Graph of the reconstructed radius for a rough object as a function of permittivity from different distances.

5. Conclusions and Future Work

The main new developments in this work are the multigrid-type scheme to handle discretizing the Lippmann-Schwinger equations in the case of large objects or through-the-wall settings and the material parameter reconstruction algorithm. Both of these processes are a significant step toward being able to solve, model, and reconstruct these scattering problems in a variety of physical situations. In particular, we have shown how these methods, especially the reconstruction algorithm, has the potential to be used to identify objects from their scattered data in a real-life scenario. We do note that there were significant restrictions applied to the type of data used here to generate these results, and these would need to be removed or reduced before the method could be applied to physical situations. In addition, there are many other methods that achieve similar results (geometric optics or physical optics), and further work would need to be done to compare this method to these others.

There are many paths for future development from here. First of all, a fair amount of this algorithm can be used in the through-the-wall setting. The scattering data can be generated using the multigrid setup, and then the reciprocity gap functional should be able to be used to reconstruct the support as before. This is technically outside of the conditions of the method as presented in previous work, but numerical experiments show that it has the potential to work. Determining the permittivity however is a more complicated matter. The walls of the room factor into the scattered field, so they would need to be taken into account when computing the predicted scattered field $\tilde{u}^s$. The thickness and permittivity of the walls could either be taken as a known parameter or potentially also be solved for in the minimization. In a physical situation, the location of the external surface of the walls could be determined before the experiment, but the rest of the parameters would be unknown.

One could also vary the situation being analyzed. For instance, if there are two objects in the room, can these methods resolve them accurately and determine each of their permittivities independently? Will there be some interaction between them that causes this to fail? If the permittivity of the object is not constant but has some additional structure, can we use a similar method to reconstruct it? In addition, it would be interesting to look into how many sources and receivers are needed to get an accurate reconstruction, both with the reciprocity gap method and with the permittivity reconstruction. For a constant permittivity and a single object, it should be able to be done with very few sources and receivers, but if you add more variability, you will likely need more.

Another avenue for future research is in analyzing how the accuracy of the reconstruction depends on the object location and how varying other parameters of the setup can affect this. From the experimental results, the object needs to be centered among the sources and receivers in order to be reconstructed appropriately. It is possible that this effect could be reduced by moving the sources and receivers farther away from the object, more directly simulating the "far-field" data used in the original LSM. At the small scale that it was tested, we noticed that moving the sources and receivers farther away from the object did not substantially affect the reconstruction of a centered object, so if it mitigates the problem for off-center object, this could be a positive step forward for this method. Also, the fact that changing the frequency and contrast of the object affected the accuracy of the reconstruction is surprising since the LSM does not give any information about these parameters, and this provides another direction for future study.

Acknowledgments
The authors acknowledge the Office of Advanced Research Computing (OARC) at Rutgers, The State University of New Jersey for providing access to the Amarel cluster and associated research computing resources that have contributed to the results reported here (http://oarc.rutgers.edu). This research was supported by ORISE.

References

Adib, F., Hsu, C.-Y., Mau, H., Katabi, D., & Durand, F. (2015). Capturing the human figure through a wall. *ACM Transactions on Graphics*, *34*, 1–13.

Ambikasaran, S., Borges, C., Imbert-Gérard, L.-M., & Fast, L. G. (2016). Adaptive, high-order accurate discretization of the Lippman-Schwinger equation in two dimensions. *SIAM Journal of Scientific Computing*, *32*, A1770–A1787.

Cakoni, F., & Colton, D. (2014). *A qualitative approach to inverse scattering theory*: 188 of Applied Mathematical Sciences Springer US.

Cakoni, F., Colton, D., & Gintides, D. (2010). The interior transmission eigenvalue problem. *SIAM Journal of Mathematical Analysis*, *42*, 2912–2921.

Cakoni, F., Colton, D., & Haddar, H. (2016). *Inverse scattering theory and transmission eigenvalues*: volume 88 of CBMS-NSF regional conference series in applied mathematics Society for Industrial and Applied Mathematics.

Charnley, M., & Wood, A. (2016). Through-the-wall radar detection analysis via numerical modeling of Maxwell's equations. *Journal of Computational Physics*, *313*, 532–548.

Charnley, M., & Wood, A. (2017). A linear sampling method for through-the-wall radar detection. *Journal of Computational Physics*, *347*, 147–159.

Colton, D., & Haddar, H. (2005). An application of the reciprocity gap functional to inverse scattering theory. *Inverse Problems*, *21*, 383–398.

Giovanni, G., & Haddar, H. (2012). Computing estimates on material properties from transmission eigenvalues. *Inverse Problems*, *28*, 055009.

Keith, S. R. (2013). Discrimination between child and adult forms using radar frequency signature analysis. Air Force Institute of Technology, AFIT-ENP-13-M-20, 2013.

Kress, R. (2010). *Linear integral equations*, Applied Mathematical Sciences (Vol. 82). New York: Springer-Verlag.

Zhao, M., Li, T., Alsheikh, M. A., Tian, Y., Zhao, H., Torralba, A., & Katabi, D. (2018). Through-wall human pose estimation using radio signals. Computer Vision and Pattern Recognition.